Resolution Guarantees in Electrical Impedance Tomography

Bastian Harrach, Marcel Ullrich

***Abstract*—Electrical impedance tomography (EIT) uses current-voltage measurements on the surface of an imaging subject to detect conductivity changes or anomalies. EIT is a promising new technique with great potential in medical imaging and non-destructive testing. However, in many applications, EIT suffers from inconsistent reliability due to its enormous sensitivity to modeling and measurement errors.**

In this work, we show that it is principally possible to give rigorous resolution guarantees in EIT even in the presence of systematic and random measurement errors. We derive a constructive criterion to decide whether a desired resolution can be achieved in a given measurement setup.

Our results cover the case where anomalies of a known minimal contrast in a subject with imprecisely known background conductivity are to be detected from noisy measurements on a number of electrodes with imprecisely known contact impedances. The considered settings are still idealized in the sense that the shape of the imaging subject has to be known and the allowable amount of uncertainty is rather low. Nevertheless, we believe that this may be a starting point to identify new applications and to design and optimize measurement setups in EIT.

***Index Terms*—Electrical impedance tomography (EIT), anomaly detection, inclusion detection, complete electrode model, resolution guarantee, monotonicity method.**

I. Introduction

ELECTRICAL impedance tomography (EIT) is an imaging technique that uses current-voltage measurements on the surface of a conductive subject to image its inner conductivity distribution. From this conductivity image, one can extract information about the physiological composition of the subject. An upcoming application of EIT is lung monitoring. Since an inflated lung has a lower specific conductivity than surrounding body tissues, this leads to a visible contrast in the EIT image. In this work, we will focus on another promising application, which is the detection of anomalies (aka inclusions) where the conductivity significantly differs from an expected background value. There are several relevant practical scenarios, e.g. the detection of tumors or hemorrhages in surrounding homogeneous tissue that has a certain conductivity contrast.

For a further overview of practical applications of EIT appearing in the fields of medical imaging and material testing of industrial or building materials, cf. e.g., [1]–[15].

B. Harrach (birth name: Bastian Gebauer) is with the Department of Mathematics, University of Stuttgart, Germany e-mail: harrach@math.uni-stuttgart.de

M. Ullrich is with the Department of Mathematics, University of Stuttgart, Germany e-mail: marcel.ullrich@mathematik.uni-stuttgart.de

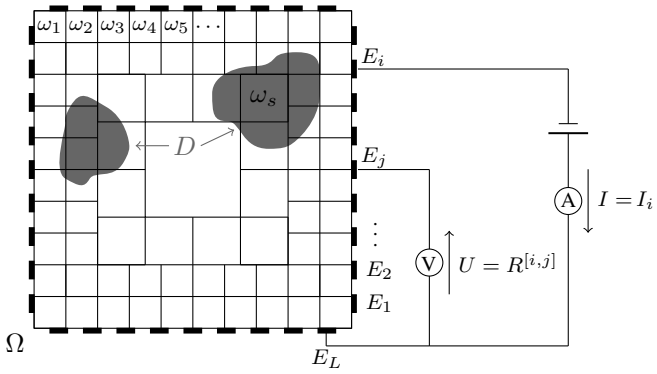

Fig. 1. Measurement setting with inclusions D occupying a subset of a subject Ω that is decomposed into a partition of subsets $\omega_1, \omega_2, \ldots \subseteq \Omega$. Driving a current through the i-th and the L-th electrode, we measure the corresponding voltage $R^{[i,j]}$ (in mV per applied mA) between the j-th and the L-th electrode. Repeating this for all i and j we obtain the measurement matrix $R = (R^{[i,j]})_{i,j=1,\ldots,L-1} \in \mathbb{R}^{(L-1)\times(L-1)}$.

The reconstruction process in EIT suffers from the fundamental ill-posedness of the underlying mathematical inverse problem which leads to an enormous sensitivity to modeling and measurement errors. Due to these inherent instability issues, high resolution EIT imaging remains an extremely challenging topic. However, several applications would already greatly benefit from low resolution EIT images, e.g. in the field of the aforementioned tumor or hemorrhage detection. For these applications, fast and low-cost monitoring techniques have to be developed in order to decide which patients should undergo more extensive diagnosis. For this task, the main concern seems to be the reliability of EIT images.

In this work, we show that it is principally possible to give rigorous resolution guarantees in EIT even in the presence of systematic and random measurement errors. Consider a measurement setting as in figure 1 where voltage-current measurements are taken on a number of electrodes attached to the boundary of an imaging domain Ω. The aim is to detect whether the domain contains one or several anomalies where the conductivity differs from some normal background range.

We describe a desired *resolution* by a partition of Ω into disjoint subsets $\omega_1, \omega_2, \ldots \subseteq \Omega$. We say that a *resolution guarantee* holds if the measured data contains enough information to

(a) correctly mark every element ω_s that is completely covered by an anomaly,
(b) correctly mark no element, if there is no anomaly at all.

In other words, a resolution guarantee ensures that no false positives are detected in the anomaly-free case, and no false negatives are detected in the case of inclusions over a certain size. Let us stress that in this work we aim to characterize the resolution up to which an anomaly can be detected. Assumptions (a) and (b) do not guarantee that the shape of a detected anomaly can be correctly determined up to a certain resolution. In that sense, the subject of this work might be called a (resolution-based) detection guarantee.

Whether a certain desired resolution can be guaranteed will depend on a number of facts, including the number and position of electrodes, the measurement pattern, the inclusion contrast, and modeling and measurement errors. The aim of this work is to derive a validation criterion to evaluate whether a desired resolution can be guaranteed. We also describe a simple reconstruction algorithm that implements (a) and (b) above.

Let us comment on the vast literature on identifiability in EIT. In the last decades, great theoretical progress has been made on the question whether two arbitrary conductivities can be distinguished by idealized noise-free and continuous measurements (the *Calderón-Problem* [16], [17]). We refer to the seminal works [18]–[21], the overview [22] and the recent breakthroughs for partial boundary data [23], [24]. The distinguishability of conductivities from finite precision data has been studied in the works of Bates, Gençer, Gisser, Ider, Isaacson, Kuzuoglu, Lionheart, Newell, Seagar, Paulson, Pidcock and Yeo [25]–[31]. Also, let us refer to a recent result of Winkler and Rieder [32] on optimal resolution meshes and to the works of Kolehmainen, Lassas, Nissinen, Ola and Kaipio [33], [34] regarding uncertainties in the subject's shape and electrode's contact impedances.

Several reconstruction methods have been proposed for anomaly or inclusion detection problems, cf., e.g., Potthast [35] for an overview. Arguably, the most prominent inclusion detection method is the Factorization Method (FM) of Kirsch, Brühl and Hanke [36]–[38], see [14], [39]–[54] for the devolopment of the FM in the field of EIT and [55] for a recent overview. Notably, in the overview [55], the FM is formulated on the basis of monotonicity-based arguments, and the recent result [56] indicates that, for EIT, the FM can be outperformed by monotonicity-based methods first formulated by Tamburrino and Rubinacci in [57], [58], see also Tamburrino, Ventre and Rubinacci [59] where the concept of *visible voxels* is introduced.

The main new idea of this work is to obtain rigorous resolution guarantees by treating worst-case scenarios with monotonicity-based ideas. To the knowledge of the authors, the results derived herein are the firsts to rigorously quantify the achievable resolution in the case of realistic electrode measurements in a setting with imprecisely known background conductivity, contact impedances and measurement noise. We believe that this will be useful for designing reliable EIT systems. Our results may be used to determine whether a desired resolution can be achieved and to quantify the required measurement accuracy. Moreover, our results could be the basis of optimization strategies regarding the resolution, or the number and positions of electrodes and the driving patterns.

The paper is organized as follows. The measurement setting including systematic and random errors is introduced in section II. Section III presents a monotonicity relation and motivates how this relation can be used to design inclusion detection methods. In section IV, we introduce the concept of a rigorous resolution guarantee and show how to verify such guarantees by a simple test. We also derive fast linearized versions of our tests that allow faster verifications at the price of underestimating the achievable resolution. Section V presents some numerical results for the verification of resolution guarantees of section IV. Section VI contains some concluding remarks.

II. The Setting

The current-voltage measurements can be modeled by the complete electrode model (CEM) as follows (cf. [60]). Let $\Omega \subseteq \mathbb{R}^n$ be a bounded domain with piecewise smooth boundary representing the conductive object and let $\sigma : \Omega \to \mathbb{R}$ be the real valued conductivity distribution inside Ω. We assume that σ and $1/\sigma$ are positive and bounded functions.

Electrodes are attached to the boundary of the object as in figure 1. Their location is denoted with $E_1, E_2, \ldots, E_L \subseteq \partial\Omega$, and their contact impedances are denoted by a vector with positive entries

$$z := \left(z^{[1]}, \ldots, z^{[L]}\right) \in \mathbb{R}^L.$$

The electrodes are assumed to be perfectly conductive.

For each $i \in \{1, 2, \ldots, L-1\}$, we drive a current I_i with strength 1 mA through the i-th electrode while keeping the L-th electrode grounded and all other electrodes insulated (so that the current flows through the grounded L-th electrode). Then the potential u_i inside Ω and the potentials $U_i = \left(U_i^{[1]}, \ldots, U_i^{[L]}\right)$ on the electrodes fulfill

$$\nabla \cdot \sigma \nabla u_i = 0 \quad \text{in } \Omega,$$

with boundary conditions

$$\int_{E_l} \sigma \left(\nabla u_i\right) \cdot \nu \, \mathrm{d}S = \delta_{l,i} - \delta_{l,L},$$
$$u_i|_{E_l} + z^{[l]} \sigma \left(\nabla u_i\right) \cdot \nu|_{E_l} = \text{const.} =: U_i^{[l]}$$

for $l \in \{1, 2, \ldots, L\}$,

$$\sigma \left(\nabla u_i\right) \cdot \nu = 0 \quad \text{on} \quad \partial\Omega \setminus \bigcup_{l=1}^{L} E_l,$$

and $U_i^{[L]} = 0$. ν is the outer normal on the boundary of Ω.

For each injected current, we measure the voltage on E_1,...,E_{L-1} against the grounded L-th electrode. We thus collect a matrix of measurements

$$R(\sigma, z) := \left(R^{[i,j]}(\sigma, z)\right)_{i,j=1}^{L-1} := \left(U_i^{[j]}\right)_{i,j=1}^{L-1} \in \mathbb{R}^{(L-1)^2}. \tag{1}$$

The matrix $R(\sigma, z)$ is easily shown to be symmetric.

We consider anomaly detecting problems where we try to detect regions (the so-called inclusions) in Ω where the conductivity differs from a normal background range. To allow

for modeling and measurement errors in this context, we make the following setting assumptions:

(a) **Conductivity distribution $\sigma(x)$:** The true conductivity distribution is given by an inclusion conductivity $\sigma_D(x)$ inside an inclusion D and by a background conductivity $\sigma_B(x)$ inside $\Omega \setminus D$, i.e.

$$\sigma(x) = \begin{cases} \sigma_D(x), & x \in D, \\ \sigma_B(x), & x \in \Omega \setminus D. \end{cases}$$

(b) **Background error $\epsilon \geq 0$:** The background conductivity approximately agrees with a known positive constant $\sigma_0 > 0$,

$$|\sigma_B(x) - \sigma_0| \leq \epsilon \quad \forall x \in \Omega \setminus D.$$

(c) **Inclusion conductivity contrast $c > 0$:** We assume that we know a lower bound on the inclusion contrast, i.e., that we know $c > 0$ with either

(i) $\sigma_D(x) - \sigma_0 \geq c \quad \forall x \in D$,
(ii) $\sigma_0 - \sigma_D(x) \geq c \quad \forall x \in D$.

(d) **Contact impedances error $\gamma \geq 0$:** We assume that we approximately know the contact impedances vector z, i.e. that we know $z_0 \in \mathbb{R}^L$ with

$$\left| z^{[l]} - z_0^{[l]} \right| \leq \gamma \quad \forall l \in \{1, 2, \ldots, L-1\}.$$

(e) **Measurement noise $\delta \geq 0$:** We assume that we can measure the voltages $R(\sigma, z)$ up to a noise level $\delta > 0$, i.e., that we are given $R_\delta \in \mathbb{R}^{(L-1)\times(L-1)}$ with

$$\|R(\sigma, z) - R_\delta\| \leq \delta.$$

Possibly replacing R_δ by its symmetric part, we can assume that R_δ is symmetric.

III. Monotonicity

Our results are based on the following monotonicity relations that extend results of Gisser, Ikehata, Isaacson, Kang, Newell, Rubinacci, Seo, Sheen, and Tamburrino [29], [57], [61], [62].

Theorem 1. *For $i \in \{1, 2\}$, let $\sigma_i : \Omega \to \mathbb{R}$ be a conductivity distribution and $z_i \in \mathbb{R}^L$ be a contact impedances vector. Then*

$$\sigma_1 \leq \sigma_2, z_1 \geq z_2 \quad \textit{implies} \quad R(\sigma_1, z_1) \geq R(\sigma_2, z_2). \quad (2)$$

The inequalities on the left side of the implication are meant pointwise. The inequality on the ride side is to be understood in the sense of matrix definiteness.

Proof. This follows from the more general theorem 2 below. □

Theorem 1 yields monotonictiy-based inclusion detection methods, cf. [57]. To present the main idea, consider the simple example where $\sigma = 1 + \chi_D$, where χ_D is the characteristic function on D, and the contact impedances vector $z \in \mathbb{R}^L$ is known exactly.

For a small ball $B \subseteq \Omega$ we define a test conductivity $\tau_B = 1 + \chi_B$. From the monotonicity relation of theorem 1 we have that

$$B \subseteq D \quad \text{implies} \quad R(\tau_B, z) \geq R(\sigma, z).$$

Hence, the union of all test balls B fulfilling $R(\tau_B, z) \geq R(\sigma, z)$ is an upper bound of the inclusion D.

In the recent work [56], the authors showed that, for continuous boundary data, monotonicity methods are actually capable of reconstructing the exact shape D under rather general assumptions. Moreover, [56] shows how to replace the monotonicity tests by fast linearized versions without losing shape information, see also [63].

We cannot expect exact shape reconstruction in settings with a finite number of electrodes and imprecisely known contact impedances and background conductivities. However, monotonicity-based arguments will allow us to characterize the achievable resolution in such settings. For this, we formulate a quantitative version of theorem 1:

Theorem 2. *For $i \in \{1, 2\}$, let $\sigma_i : \Omega \to \mathbb{R}$ be a conductivity distribution and $z_i \in \mathbb{R}^L$ be a contact impedances vector. Given $w \in \mathbb{R}^{L-1}$, let (v_i, V_i) be the corresponding potentials resulting from driving a current of w_j through the j-th electrode, respectively. (Note that this implies a current flux of $-\sum_{l=1}^{L} w_l$ through the grounded L-th electrode.) Then,*

$$\begin{aligned} &\int_\Omega (\sigma_1 - \sigma_2) |\nabla v_2|^2 \, \mathrm{d}x \\ &+ \sum_{l=1}^{L} \left(\frac{1}{z_1^{[l]}} - \frac{1}{z_2^{[l]}} \right) \int_{E_l} \left(v_2 - V_2^{[l]} \right)^2 \mathrm{d}s \\ &\geq w^T \left(R(\sigma_2, z_2) - R(\sigma_1, z_1) \right) w \\ &\geq \int_\Omega \frac{\sigma_2}{\sigma_1} (\sigma_1 - \sigma_2) |\nabla v_2|^2 \, \mathrm{d}x \\ &\quad + \sum_{l=1}^{L} \frac{z_1^{[l]}}{z_2^{[l]}} \left(\frac{1}{z_1^{[l]}} - \frac{1}{z_2^{[l]}} \right) \int_{E_l} \left(v_2 - V_2^{[l]} \right)^2 \mathrm{d}s. \end{aligned}$$

Proof. From the variational formulation of the CEM (cf., e.g., [60]), we obtain for $i, j \in \{1, 2\}$,

$$\begin{aligned} w^T V_j &= \int_\Omega \sigma_i \nabla v_i \cdot \nabla v_j \mathrm{d}x \\ &\quad + \sum_{l=1}^{L} \frac{1}{z_i^{[l]}} \int_{E_l} \left(v_i - V_i^{[l]} \right) \left(v_j - V_j^{[l]} \right) \mathrm{d}s \\ &=: B_i((v_i, V_i), (v_j, V_j)). \end{aligned}$$

and, by linearity, we have that

$$V_j = R(\sigma_j, z_j) w, \quad j \in \{1, 2\}.$$

Hence, it holds that

$$\begin{aligned}
&w^T \left(R\left(\sigma_2, z_2\right) - R\left(\sigma_1, z_1\right)\right) w \\
&= w^T \left(V_2 - V_1\right) \\
&= 2B_1\left(\left(v_1, V_1\right), \left(v_2, V_2\right)\right) - B_2\left(\left(v_2, V_2\right), \left(v_2, V_2\right)\right) \\
&\quad - B_1\left(\left(v_1, V_1\right), \left(v_1, V_1\right)\right) \\
&= -\int_\Omega \sigma_1 \left|\nabla\left(v_1 - v_2\right)\right|^2 \mathrm{d}x \\
&\quad - \sum_{l=1}^{L} \frac{1}{z_1^{[l]}} \int_{E_l} \left(\left(v_1 - V_1^{[l]}\right) - \left(v_2 - V_2^{[l]}\right)\right)^2 \mathrm{d}s \\
&\quad + \int_\Omega \left(\sigma_1 - \sigma_2\right) \left|\nabla v_2\right|^2 \mathrm{d}x \\
&\quad + \sum_{l=1}^{L} \left(\frac{1}{z_1^{[l]}} - \frac{1}{z_2^{[l]}}\right) \int_{E_l} \left(v_2 - V_2^{[l]}\right)^2 \mathrm{d}s.
\end{aligned}$$

Since the first two summands are non-negative, the first inequality of the theorem follows.

Interchanging the pairs (σ_1, z_1) and (σ_2, z_2) and applying

$$\begin{aligned}
&\sigma_2 \left|\nabla\left(v_2 - v_1\right)\right|^2 + \left(\sigma_1 - \sigma_2\right) \left|\nabla v_1\right|^2 \\
&= \sigma_1 \left|\nabla v_1 - \frac{\sigma_2}{\sigma_1} \nabla v_2\right|^2 + \frac{\sigma_2}{\sigma_1} \left(\sigma_1 - \sigma_2\right) \left|\nabla v_2\right|^2
\end{aligned}$$

and

$$\begin{aligned}
&\frac{1}{z_2^{[l]}} \left(\left(v_2 - V_2^{[l]}\right) - \left(v_1 - V_1^{[l]}\right)\right)^2 \\
&+ \left(\frac{1}{z_1^{[l]}} - \frac{1}{z_2^{[l]}}\right) \left(v_1 - V_1^{[l]}\right)^2 \\
&= \frac{1}{z_1^{[l]}} \left(\left(v_1 - V_1^{[l]}\right) - \frac{z_1^{[l]}}{z_2^{[l]}} \left(v_2 - V_2^{[l]}\right)\right)^2 \\
&\quad + \frac{z_1^{[l]}}{z_2^{[l]}} \left(\frac{1}{z_1^{[l]}} - \frac{1}{z_2^{[l]}}\right) \left(v_2 - V_2^{[l]}\right)^2
\end{aligned}$$

yields

$$\begin{aligned}
&w^T \left(R\left(\sigma_2, z_2\right) - R\left(\sigma_1, z_1\right)\right) w \\
&= \int_\Omega \sigma_1 \left|\nabla v_1 - \frac{\sigma_2}{\sigma_1} \nabla v_2\right|^2 \mathrm{d}x + \int_\Omega \frac{\sigma_2}{\sigma_1} \left(\sigma_1 - \sigma_2\right) \left|\nabla v_2\right|^2 \mathrm{d}x \\
&\quad + \sum_{l=1}^{L} \int_{E_l} \frac{1}{z_1^{[l]}} \left(\left(v_1 - V_1^{[l]}\right) - \frac{z_1^{[l]}}{z_2^{[l]}} \left(v_2 - V_2^{[l]}\right)\right)^2 \mathrm{d}s \\
&\quad + \sum_{l=1}^{L} \int_{E_l} \frac{z_1^{[l]}}{z_2^{[l]}} \left(\frac{1}{z_1^{[l]}} - \frac{1}{z_2^{[l]}}\right) \left(v_2 - V_2^{[l]}\right)^2 \mathrm{d}s.
\end{aligned}$$

Since the last two summands are non-negative, the second inequality of the theorem is proven. □

IV. Resolution Guarantees

In this section we introduce the concept of rigorous resolution guarantees and show how to verify such guarantees by a simple test. We consider the setting described in section II.

Definition 3. *An inclusion detection method that yields a reconstruction D_R to the true inclusion D is said to fulfill a **resolution guarantee** with respect to a partition $(\omega_s)_{s=1}^N$ if*

(i) *$\omega_s \subseteq D$ implies $\omega_s \subseteq D_R$ for $s \in \{1, 2, \ldots, N\}$ (i.e., every element that is covered by the inclusion will correctly be marked in the reconstruction), and*

(ii) *$D = \emptyset$ implies $D_R = \emptyset$ (i.e., if there is no inclusion then no element will be marked in the reconstruction).*

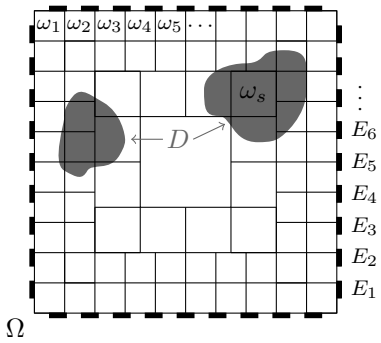

Fig. 2. Setting with a sample inclusion and resolution.

Hence, if a resolution guarantee holds true then no false positives are detected in the anomaly-free case, and no false negatives are detected in the case of inclusions over a certain size.

Obviously, a resolution guarantee will not hold true for arbitrarily fine partitions. The achievable resolution will depend on the number of electrodes, the inclusion's contrast, the background error, contact impedances error, and the measurement noise, cf. section II(a)-(e).

We will derive a simple test to verify whether a resolution guarantee holds true for a given partition. To this end, we first consider the case of inclusions that are more conductive than the background. The analogous results for less conductive inclusions are summarized in section IV-C. We use the following notations:

$$\begin{aligned}
\sigma_{B\min} &:= \sigma_0 - \epsilon, \\
\sigma_{B\max} &:= \sigma_0 + \epsilon, \\
\sigma_{D\min} &:= \sigma_0 + c, \\
z_{\min} &:= z_0 - \gamma(1, 1, \ldots, 1), \\
z_{\max} &:= z_0 + \gamma(1, 1, \ldots, 1).
\end{aligned}$$

A. Verification of resolution guarantees

To verify whether a resolution guarantee holds in a given setting, we will apply the following monotonicity-based inclusion detection method. In the following, we denote the set of eigenvalues of a symmetric square matrix A by $\mathrm{eig}(A)$ and we write $A_1 \geq A_2$ (or $A_2 \leq A_1$) if the difference $A_1 - A_2$ of two symmetric square matrices is positive definite, i.e. if $A_1 - A_2$ possesses only non-negative eigenvalues.

Algorithm 4. *Mark each resolution element ω_s for which*

$$R(\tau_s, z_{max}) + \delta \mathrm{Id} \geq R_\delta, \tag{3}$$

where

$$\tau_s := \sigma_{B\min} \chi_{\Omega \setminus \omega_s} + \sigma_{D\min} \chi_{\omega_s}, \quad s \in \{1, 2, \ldots, N\}. \tag{4}$$

Then the reconstruction D_R is given by the union of the marked resolution elements.

Theorem 5. *The reconstruction of algorithm 4 fulfils the resolution guarantee if*

$$\mu < -2\delta \leq 0 \tag{5}$$

with

$$\mu := \max_{s=1}^{N} \left(\min\left(\operatorname{eig}\left(R(\tau_s, z_{\max}) - R(\sigma_{B\max}, z_{\min})\right)\right)\right). \tag{6}$$

Proof. First, let $\omega_s \subseteq D$. Then, $\tau_s \leq \sigma$ and $z_{\max} \geq z$. Theorem 1 implies that

$$R(\sigma, z) \leq R(\tau_s, z_{\max}).$$

Hence, $R(\tau_s, z_{\max}) + \delta \mathrm{Id} \geq R_\delta$, so that ω_s will be marked by algorithm 4. This shows that part (i) of the resolution guarantee is satisfied.

To show part (ii) of the resolution guarantee, assume that $D = \emptyset$ and $D_R \neq \emptyset$. Then there must be an index $s \in \{1, 2, \ldots, N\}$ with

$$R(\tau_s, z_{\max}) + \delta \mathrm{Id} \geq R_\delta.$$

Using Theorem 1 we obtain

$$\begin{aligned} -2\delta \mathrm{Id} &\leq R(\tau_s, z_{\max}) - (\delta \mathrm{Id} + R_\delta) \\ &\leq R(\tau_s, z_{\max}) - R(\sigma, z) \\ &\leq R(\tau_s, z_{\max}) - R(\sigma_{B\max}, z_{\min}), \end{aligned}$$

and thus $\mu \geq -2\delta$. □

Theorem 5 gives a rigorous yet conceptually simple criterion to check whether a given resolution guarantee is valid or not. Given a partition $(\omega_s)_{s=1}^N$, and bounds on the background and contact impedance error, we obtain μ from calculating $R(\tau_s, z_{\max})$ and $R(\sigma_{B\max}, z_{\min})$ by solving the partial differential equations of the complete electrode model. If this yields a negative value for μ, then the resolution guarantee holds true up to a measurement error of $\delta < -\mu/2$.

B. Fast linearized verification of resolution guarantees

Checking the criterion in Theorem 5 for a partition with N elements, requires the solution of $N+1$ forward problems. A less accurate but considerably faster test can be obtained by replacing the monotonicity tests in algorithm 4

$$R(\tau_s, z_{\max}) + \delta \mathrm{Id} \geq R_\delta,$$

with their linearized approximations

$$R(\sigma_{B\min}, z_{\max}) + \lambda R'(\sigma_{B\min}, z_{\max})(\chi_{\omega_s}) + \delta \mathrm{Id} \geq R_\delta, \tag{7}$$

where $\lambda \in \mathbb{R}$ is a suitably chosen contrast level (as defined in the algorithms 7 and 11),

$$R'\left(\sigma_{B\min}, z_{\max}\right)\left(\chi_{\omega_s}\right) = -\left(\int_{\omega_s} \nabla u_i \cdot \nabla u_j \,\mathrm{d}x\right)_{i,j=1}^{L-1}, \tag{8}$$

and u_i is the solution of the complete electrode model introduced in in section II with interior conductivity $\sigma_{B\min}$ and contact impedances $z_{\max}$. One can interpret R' as the Fréchet-derivative of the measurements with respect to the interior conductivity distribution, cf., e.g., Lionheart [8] or Lechleiter and Rieder [64], but we will not require this in the following.

Remark 6. *The matrix $R'\left(\sigma_{B\min}, z_{\max}\right)\left(\chi_{\omega_s}\right)$ can be expressed in terms of the sensitivity matrix S that is frequently being used in FEM-based EIT solvers (cf., e.g., [65] for a recent work in the context of inclusion detection).*

Let $(q_r)_{r=1}^p$ be the elements of a FEM discretization of the considered domain Ω. The sensitivity matrix $S \in \mathbb{R}^{(L-1)^2 \times p}$ is given by

$$S = \begin{pmatrix} S_1 \\ \vdots \\ S_{L-1} \end{pmatrix}, \tag{9}$$

with

$$S_j = \left(S_j^{[i,r]}\right) = \left(-\int_{q_r} \nabla u_i \cdot \nabla u_j \,\mathrm{d}x\right) \in \mathbb{R}^{L-1 \times p}. \tag{10}$$

If each element ω_s in the resolution partition is a union of elements q_r of the FEM-discretization, then the entries of R' can be obtained from summing up the corresponding entries of S,

$$R'\left(\sigma_{B\min}, z_{\max}\right)\left(\chi_{\omega_s}\right) = \left(\sum_{r:\ q_r \subseteq \omega_s} S_j^{[i,r]}\right)_{i,j=1}^{L-1}. \tag{11}$$

To choose the parameter λ we require the additional knowledge of a global bound $\sigma_{\max}$ with

$$\sigma(x) \leq \sigma_{\max} \quad \forall x \in \Omega. \tag{12}$$

Algorithm 7. *Mark each resolution element ω_s for which*

$$T_s + \delta \mathrm{Id} \geq R_\delta, \tag{13}$$

where

$$T_s := R(\sigma_{B\min}, z_{\max}) + \lambda R'(\sigma_{B\min}, z_{\max})(\chi_{\omega_s}), \tag{14}$$

$$\lambda := (c + \epsilon)\frac{\sigma_{B\min}}{\sigma_{\max}}, \quad s \in \{1, 2, \ldots, N\}. \tag{15}$$

Then the reconstruction D_R is given by the union of the marked resolution elements.

Theorem 8. *The reconstruction of algorithm 7 fulfils the resolution guarantee if*

$$\mu < -2\delta \leq 0 \tag{16}$$

with

$$\mu := \max_{s=1}^{N}(\min(\operatorname{eig}(T_s - R(\sigma_{B\max}, z_{\min})))). \tag{17}$$

Proof. First, let $\omega_s \subseteq D$. Given a vector $w \in \mathbb{R}^{L-1}$, let u_w be the inner potential in a body with interior conductivity $\sigma_{B\min}$ and contact impedances $z_{\max}$ that results from driving a current of w_j through the j-th electrode, respectively.

Theorem 2 yields that

$$\begin{aligned} &w^T(R(\sigma_{B\min}, z_{\max}) - R(\sigma, z_{\max}))w \\ &\geq \int_\Omega \frac{\sigma_{B\min}}{\sigma}(\sigma - \sigma_{B\min})|\nabla u_w|^2 \mathrm{d}x, \end{aligned}$$

and since $\omega_s \subseteq D$ implies $\sigma - \sigma_{B\min} \geq (c+\epsilon)\chi_{\omega_s}$, it follows that

$$R(\sigma_{B\min}, z_{\max}) - R(\sigma, z_{\max}) \geq -\lambda R'(\sigma_{B\min}, z_{\max})(\chi_{\omega_s})$$

Hence, we obtain from theorem 1 that

$$\begin{aligned} &T_s + \delta \mathrm{Id} \\ &= R(\sigma_{B\min}, z_{\max}) + \lambda R'(\sigma_{B\min}, z_{\max})(\chi_{\omega_s}) + \delta \mathrm{Id} \\ &\geq R(\sigma, z_{\max}) + \delta \mathrm{Id} \geq R(\sigma, z) + \delta \mathrm{Id} \\ &\geq R_\delta. \end{aligned}$$

Hence, ω_s will be marked, which shows that part (i) of the resolution guarantee is satisfied.

The proof of part (ii) of the resolution guarantee is completely analogous to the proof of part (ii) in theorem 5. □

C. Verification for less conductive inclusions

The theory and the results are almost the same in the case that we consider inclusions that are less conductive than the background. In that case we set

$$\sigma_{D\max} := \sigma_0 - c < \sigma_{B\min} \tag{18}$$

and consider the following algorithm.

Algorithm 9. *Mark each resolution element ω_s for which*

$$R(\tau_s, z_{\min}) - \delta \mathrm{Id} \leq R_\delta, \tag{19}$$

where

$$\tau_s := \sigma_{B\max}\chi_{\Omega\setminus\omega_s} + \sigma_{D\max}\chi_{\omega_s}, \quad s \in \{1, 2, \ldots, N\}.$$

Then the reconstruction D_R is given by the union of the marked resolution elements.

Theorem 10. *The reconstruction of algorithm 9 fulfils the Resolution guarantee if*

$$\mu > 2\delta \geq 0 \tag{20}$$

with

$$\mu := \min_{s=1}^{N} \left(\max\left(\mathrm{eig}\left(R(\tau_s, z_{\min}) - R(\sigma_{B\min}, z_{\max})\right)\right)\right).$$

Proof. The proof of part (i) of the resolution guarantee is analogous to the proof of part (i) in theorem 5.

To show part (ii) of the resolution guarantee, assume that $D = \emptyset$ and $D_R \neq \emptyset$. Then there must be an index $i \in \{1, 2, \ldots, N\}$ with

$$R(\tau_s, z_{\min}) - \delta \mathrm{Id} \leq R_\delta \leq R(\sigma, z) + \delta \mathrm{Id}.$$

Using theorem 1 we obtain

$$R(\tau_s, z_{\min}) - 2\delta \mathrm{Id} \leq R(\sigma_{B\min}, z_{\max}),$$

and thus $\mu \leq 2\delta$. □

Algorithm 11. *Mark each resolution element ω_s for which*

$$T_s - \delta \mathrm{Id} \leq R_\delta, \tag{21}$$

where

$$T_s := R(\sigma_{B\max}, z_{\min}) + R'(\sigma_{B\max}, z_{\min})(\lambda\chi_{\omega_s}), \tag{22}$$

$$\lambda := -(c+\epsilon), \quad s \in \{1, 2, \ldots, N\}. \tag{23}$$

Then the reconstruction D_R is given by the union of the marked resolution elements.

Theorem 12. *The reconstruction of algorithm 11 fulfils the resolution guarantee if*

$$\mu > 2\delta \geq 0 \tag{24}$$

with

$$\mu := \min_{s=1}^{N} \left(\max\left(\mathrm{eig}\left(T_s - R(\sigma_{B\min}, z_{\max})\right)\right)\right). \tag{25}$$

Proof. First, let $\omega_s \subseteq D$. Given a vector $w \in \mathbb{R}^{L-1}$, let u_w be the inner potential in a body with interior conductivity $\sigma_{B\max}$ and contact impedances $z_{\min}$ that results from driving a current of w_j through the j-th electrode, respectively. As in the proof of theorem 8 we obtain by applying theorem 1 and 2:

$$w^T \left(R(\sigma_{B\max}, z_{\min}) - \delta \mathrm{Id} - R_\delta\right) w \leq \lambda \int_D |\nabla u_w|^2 \, \mathrm{d}x.$$

This yields

$$T_s - \delta \mathrm{Id} \leq R_\delta.$$

Hence, ω_s will be marked, which shows that part (i) of the resolution guarantee is satisfied.

The proof of part (ii) of the resolution guarantee is completely analogue to the proof of part (ii) in theorem 10. □

V. Numerical results

The numerical results in this section are generated with MATLAB® and the commercial FEM-software COMSOL®.

In all examples, we used the measurement setup explained in figure 1. Conductivities and contact impedances are given in Siemens/meter (S/m) and Ohmsquaremeter (Ωm^2), respectively. The unit of length is meter (m). Currents and voltages are measured in milliampere (mA) and millivolt (mV), respectively.

A. Results for academic examples

We consider two measurement setups (see fig. 3 and 4). For both settings, we assume that the background conductivity is approximately $\sigma_0 = 1$ and the contact impedances are approximately $z_0 = (1, 1, \ldots, 1) \in \mathbb{R}^L$. The inclusions conductivity contrast is assumed to be $c = 10$.

The results for figure 3 using our non-linearised verification procedure in theorem 5 are presented in table I. Table II shows the results for figure 3 obtained from the linearized verification procedure in theorem 8 under the additional assumption that $\sigma_{D\max} = 15$ is an upper bound on the inclusion contrast.

TABLE I
RG validation for figure 3 (non-linearized).

background error ϵ:	contact imped. error γ:	abs. meas. noise δ:
0%	0%	0.13
0.25%	0%	0.11
0%	0.25%	0.10
0.25%	0.25%	0.088

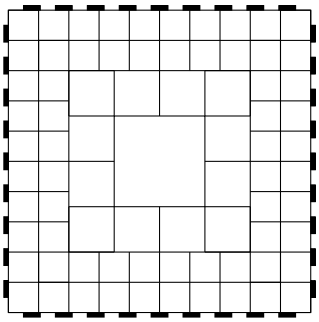

Fig. 3. $\Omega = [-1,1]^2$ and 36 electrodes are covering 50% of the boundary. The first electrode E_1 is the lowermost one on the right boundary edge and the electrodes are numbered counter-clockwise.

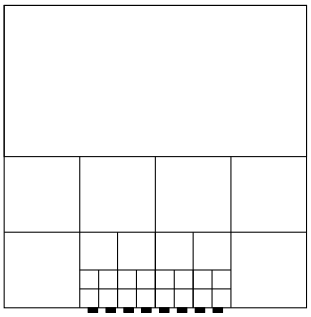

Fig. 4. $\Omega = [-1,1]^2$ and 8 electrodes are covering 25% of the lower boundary edge. The electrodes are numbered from the left to the right.

TABLE II
RG VALIDATION FOR FIGURE 3 (LINEARIZED).

background error ϵ:	contact imped. error γ:	abs. meas. noise δ:
0%	0%	0.051
0.25%	0%	0.035
0%	0.25%	0.025
0.25%	0.25%	0.013

The desired resolution shown in the second measurement setup in figure 4 is particularly ambitious. Using the non-linearised verification method it is not possible to guarantee the shown resolution. Under the additional assumption $\sigma_{D\max} = 12$ on the upper bound of the inclusion contrast, the resolution can be guaranteed using the linearized validation method up to the errors given in table III.

TABLE III
RG VALIDATION FOR FIGURE 4 (LINEARIZED).

background error ϵ:	contact imped. error γ:	abs. meas. noise δ:
0%	0%	0.026
0.05%	0%	0.022
0%	0.05%	0.0036
0.05%	0.05%	0.0022

B. Results using physiologically relevant parameters

The following setting is motivated by the idea of detecting hemorrhages inside fatty tissue. The resolution partition and the electrodes are concentrated to the lower half of a circle-shaped object Ω. We used physiological parameter values based on the overview about electric properties of tissue [66]. We assume that the background conductivity is approximately $\sigma_0 = 0.03$. The inclusion minimal conductivity contrast is $c = 0.43 - 0.03 = 0.4$ and the upper bound of the inclusion conductivity is $\sigma_{D\max} = 0.7$.

Since realistic values for contact impedances are typically much smaller than 1 (cf. [67]), we assume the contact impedance on each electrode to be approximately 0.01.

The results for figure 5 using our non-linearized verification procedure in theorem 5 are presented in table IV. Table V shows the results for figure 5 obtained from the linearized verification procedure in theorem 8.

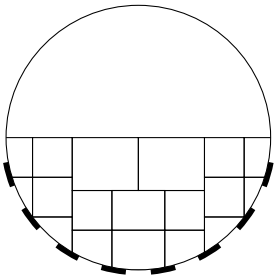

Fig. 5. Ω is a disk with diameter of 0.05 and 8 electrodes are covering 47% of the lower half of the boundary. The electrodes are numbered from the left to the right. The resolution partition covers the lower half of the disk.

TABLE IV
RG VALIDATION FOR FIGURE 5 (NON-LINEARIZED)

background error ϵ:	contact imped. error γ:	abs. meas. noise δ:
0%	0%	4.4
5%	0%	0.7
0%	5%	4.1
5%	5%	0.6

TABLE V
RG VALIDATION FOR FIGURE 5 (LINEARIZED)

background error ϵ:	contact imped. error γ:	abs. meas. noise δ:
0%	0%	1.8
1%	0%	0.7
0%	1%	1.8
1%	1%	0.7

C. Reconstruction guarantees in a region of interest

Our results can be extended to the case where certain areas should be excluded from the region of interest, e.g., if their background range is known to be violated. As an example, we will add to the setting in section V-B an area ω_I consisting of bone and blood beside fat with a conductivity range of $(0.01, 0.7)$, cf. [66].

The theory in IV-A can be extended as follows: Let

$$\sigma(x) \in (\sigma_{I\min}, \sigma_{I\max}) \quad \forall x \in \omega_I$$

be the bounds for the conductivity in the area that is to be excluded from the region of interest. We apply algorithm 4 with the following changes: τ_s in (4) is replaced by

$$\tau_s := \sigma_{B\min}\chi_{\Omega\setminus(\omega_s\cup\omega_I)} + \sigma_{D\min}\chi_{\omega_s} + \sigma_{I\min}\chi_{\omega_I} \tag{26}$$

and $\sigma_{B\max}$ in (6) is replaced by

$$\sigma_{B\max}\chi_{\Omega\setminus\omega_I} + \sigma_{I\max}\chi_{\omega_I}. \tag{27}$$

Then, analogously to the result in theorem 5, we obtain a reconstruction guarantee where every element covered by the inclusion will be correctly marked, and no element will be marked if there is no anomaly outside of ω_I.

We tested this variant on the setting shown in figure 6 where ω_I is assumed to consist of bone and blood beside fat with a conductivity range of $(0.01, 0.7)$. The results are presented in table VI.

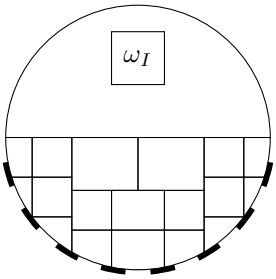

Fig. 6. Ω is a disk with diameter of 0.05 and 8 electrodes are covering 47% of the lower half of the boundary. The electrodes are numbered from the left to the right. The resolution partition covers the lower half of the disk. The area ω_I allows the presence of bone and blood beside fat.

TABLE VI
RG (EXTENDED VERSION) VALIDATION FOR FIGURE 6

background error ϵ:	contact imped. error γ:	abs. meas. noise δ:
0%	0%	2.6
5%	0%	0.3
0%	5%	2.4
5%	5%	0.2

VI. Conclusion and discussion

We have introduced a rigorous concept of resolution for anomaly detection and showed that it is principally possible to rigorously guarantee a certain resolution even for settings that include both, systematic modeling (background and contact impedance) errors and general (e.g., measurement) errors.

We have derived a constructive method to evaluate the amount of errors up to which a given desired resolution can be guaranteed. We have also derived a linearized variant of our method that allows fast validation of resolution guarantees (while still yielding rigorous results). In that context let us stress that somewhat surprisingly the linearized variant does not seem to be always inferior to the non-linearized variant as the last example in section V shows.

Our results may be used to determine whether a desired resolution can be achieved and to quantify the required measurement accuracy. Moreover, our results could be the basis of optimization strategies regarding the resolution, or the number and positions of electrodes and the driving patterns.

It would be interesting to extend our approach to explicitly address other systematic errors, e.g. including the imaging domain shape and the electrodes position.

We believe that further investigation and experimental justification of the concept of resolution guarantees could help improving the reliability of EIT-based anomaly detection.

VII. Acknowledgements

The authors would like to thank the German Research Foundation (DFG) for financial support of the project within the Cluster of Excellence in Simulation Technology (EXC 310/1) at the University of Stuttgart.

References

[1] D. Barber and B. Brown, "Applied potential tomography," *J. Phys. E: Sci. Instrum.*, vol. 17, no. 9, pp. 723–733, 1984.
[2] A. Wexler, B. Fry, and M. Neuman, "Impedance-computed tomography algorithm and system," *Applied optics*, vol. 24, no. 23, pp. 3985–3992, 1985.
[3] J. Newell, D. G. Gisser, and D. Isaacson, "An electric current tomograph," *IEEE Trans. Biomed. Eng.*, vol. 35, no. 10, pp. 828–833, 1988.
[4] P. Metherall, D. Barber, R. Smallwood, and B. Brown, "Three dimensional electrical impedance tomography," *Nature*, vol. 380, no. 6574, pp. 509–512, 1996.
[5] M. Cheney, D. Isaacson, and J. C. Newell, "Electrical impedance tomography," *SIAM Rev.*, vol. 41, no. 1, pp. 85–101, 1999.
[6] L. Borcea, "Electrical impedance tomography," *Inverse problems*, vol. 18, no. 6, pp. R99–R136, 2002.
[7] ——, "Addendum to 'Electrical impedance tomography'," *Inverse Problems*, vol. 19, no. 4, pp. 997–998, 2003.
[8] W. R. B. Lionheart, "EIT reconstruction algorithms: pitfalls, challenges and recent developments," *Physiol. Meas.*, vol. 25, pp. 125–142, 2004.
[9] D. Holder, *Electrical Impedance Tomography: Methods, History and Applications*. Bristol, UK: IOP Publishing, 2005.
[10] R. Bayford, "Bioimpedance tomography (electrical impedance tomography)," *Annu. Rev. Biomed. Eng.*, vol. 8, pp. 63–91, 2006.
[11] M. H. Choi, T.-J. Kao, D. Isaacson, G. Saulnier, and J. C. Newell, "A reconstruction algorithm for breast cancer imaging with electrical impedance tomography in mammography geometry," *IEEE Trans. Biomed. Eng.*, vol. 54, no. 4, pp. 700–710, 2007.
[12] R. J. Halter, A. Hartov, and K. D. Paulsen, "A broadband high-frequency electrical impedance tomography system for breast imaging," *IEEE Trans. Med. Imaging*, vol. 55, no. 2, pp. 650–659, 2008.
[13] F. S. Moura, J. C. C. Aya, A. T. Fleury, M. B. P. Amato, and R. G. Lima, "Dynamic imaging in electrical impedance tomography of the human chest with online transition matrix identification," *IEEE Trans. Biomed. Eng.*, vol. 57, no. 2, pp. 422–431, 2010.
[14] A. Adler, R. Gaburro, and W. Lionheart, "Electrical impedance tomography," in *Handbook of Mathematical Methods in Imaging*. Springer, 2011, pp. 599–654.
[15] O. G. Martinsen and S. Grimnes, *Bioimpedance and bioelectricity basics*. Academic press, 2011.
[16] A. P. Calderón, "On an inverse boundary value problem," in *Seminar on Numerical Analysis and its Application to Continuum Physics*, W. H. Meyer and M. A. Raupp, Eds. Rio de Janeiro: Brasil. Math. Soc., 1980, pp. 65–73.
[17] ——, "On an inverse boundary value problem," *Comput. Appl. Math.*, vol. 25, no. 2–3, pp. 133–138, 2006.
[18] R. Kohn and M. Vogelius, "Determining conductivity by boundary measurements," *Comm. Pure Appl. Math.*, vol. 37, no. 3, pp. 289–298, 1984.
[19] R. V. Kohn and M. Vogelius, "Determining conductivity by boundary measurements II. interior results," *Comm. Pure Appl. Math.*, vol. 38, no. 5, pp. 643–667, 1985.
[20] A. I. Nachman, "Global uniqueness for a two-dimensional inverse boundary value problem," *Ann. of Math.*, pp. 71–96, 1996.
[21] K. Astala and L. Päivärinta, "Calderón's inverse conductivity problem in the plane," *Ann. of Math.*, pp. 265–299, 2006.

[22] G. Uhlmann, "Commentary on Calderóns paper (29) On an inverse boundary value problem," *Selected papers of Alberto P. Calderón*, pp. 623–636, 2008.

[23] O. Y. Imanuvilov, G. Uhlmann, and M. Yamamoto, "Determination of second-order elliptic operators in two dimensions from partial Cauchy data," *Proc. Natl. Acad. Sci. USA*, vol. 108, no. 2, pp. 467–472, 2011.

[24] C. E. Kenig and M. Salo, "Recent progress in the Calderón problem with partial data," *Contemp. Math.(to appear)*, 2013.

[25] A. Seagar, T. Yeo, and R. Bates, "Full-wave computed tomography. Part 2: Resolution limits," *IEE Proceedings*, vol. 131, no. 8, pp. 616–622, 1984.

[26] A. Seagar and R. Bates, "Full-wave computed tomography. Part 4: Low-frequency electric current CT," *IEE Proceedings*, vol. 132, no. 7, pp. 455–466, 1985.

[27] D. Isaacson, "Distinguishability of conductivities by electric current computed tomography," *IEEE Trans. Med. Imaging*, vol. 5, no. 2, pp. 91–95, 1986.

[28] D. Gisser, D. Isaacson, and J. Newell, "Current topics in impedance imaging," *Clin. Phys. Physiol. Meas.*, vol. 8, no. 4A, p. 39, 1987.

[29] ——, "Electric current computed tomography and eigenvalues," *SIAM J. Appl. Math.*, vol. 50, no. 6, pp. 1623–1634, 1990.

[30] K. Paulson, W. Lionheart, and M. Pidcock, "Optimal experiments in electrical impedance tomography," *IEEE Trans. Med. Imaging*, vol. 12, no. 4, pp. 681–686, 1993.

[31] N. Gençer, M. Kuzuoglu, and Y. Ider, "Electrical impedance tomography using induced currents," *IEEE Trans. Med. Imaging*, vol. 13, no. 2, pp. 338–350, 1994.

[32] R. Winkler and A. Rieder, "Resolution-controlled conductivity discretization in electrical impedance tomography," *SIAM J. Imaging Sciences*, vol. 7, no. 4, pp. 2048–2077, 2014.

[33] V. Kolehmainen, M. Lassas, and P. Ola, "Electrical impedance tomography problem with inaccurately known boundary and contact impedances," *IEEE Trans. Med. Imaging*, vol. 27, no. 10, pp. 1404–1414, 2008.

[34] A. Nissinen, V. Kolehmainen, and J. P. Kaipio, "Compensation of modelling errors due to unknown domain boundary in electrical impedance tomography," *IEEE Trans. Med. Imaging*, vol. 30, no. 2, pp. 231–242, 2011.

[35] R. Potthast, "A survey on sampling and probe methods for inverse problems," *Inverse Problems*, vol. 22, p. R1, 2006.

[36] A. Kirsch, "Characterization of the shape of a scattering obstacle using the spectral data of the far field operator," *Inverse Problems*, vol. 14, pp. 1489–1512, 1998.

[37] M. Brühl and M. Hanke, "Numerical implementation of two noniterative methods for locating inclusions by impedance tomography," *Inverse Problems*, vol. 16, pp. 1029–1042, 2000.

[38] M. Brühl, "Explicit characterization of inclusions in electrical impedance tomography," *SIAM J. Math. Anal.*, vol. 32, no. 6, pp. 1327–1341, 2001.

[39] M. Hanke and M. Brühl, "Recent progress in electrical impedance tomography," *Inverse Problems*, vol. 19, no. 6, pp. S65–S90, 2003.

[40] N. Hyvönen, "Complete electrode model of electrical impedance tomography: Approximation properties and characterization of inclusions," *SIAM J. Appl. Math.*, vol. 64, no. 3, pp. 902–931, 2004.

[41] A. Kirsch, "The factorization method for a class of inverse elliptic problems," *Math. Nachr.*, vol. 278, no. 3, pp. 258–277, 2005.

[42] B. Gebauer, "The factorization method for real elliptic problems," *Z. Anal. Anwend.*, vol. 25, no. 1, pp. 81–102, 2006.

[43] B. Gebauer and N. Hyvönen, "Factorization method and irregular inclusions in electrical impedance tomography," *Inverse Problems*, vol. 23, no. 5, p. 21592170, 2007.

[44] N. Hyvonen, H. Hakula, and S. Pursiainen, "Numerical implementation of the factorization method within the complete electrode model of electrical impedance tomography," *Inverse Probl. Imaging*, vol. 1, no. 2, pp. 299–317, 2007.

[45] A. I. Nachman, L. Päivärinta, and A. Teirilä, "On imaging obstacles inside inhomogeneous media," *J. Funct. Anal.*, vol. 252, no. 2, pp. 490–516, 2007.

[46] B. Gebauer, "Localized potentials in electrical impedance tomography," *Inverse Probl. Imaging*, vol. 2, no. 2, pp. 251–269, 2008.

[47] M. Hanke and B. Schappel, "The factorization method for electrical impedance tomography in the half-space," *SIAM J. Appl. Math.*, vol. 68, no. 4, pp. 907–924, 2008.

[48] A. Kirsch and N. Grinberg, *The Factorization Method for Inverse Problems*, ser. Oxford Lecture Ser. Math. Appl. Oxford: Oxford University Press, 2008, vol. 36.

[49] A. Lechleiter, N. Hyvönen, and H. Hakula, "The factorization method applied to the complete electrode model of impedance tomography," *SIAM J. Appl. Math.*, vol. 68, no. 4, pp. 1097–1121, 2008.

[50] H. Hakula and N. Hyvönen, "On computation of test dipoles for factorization method," *BIT*, vol. 49, no. 1, pp. 75–91, 2009.

[51] B. Harrach and J. K. Seo, "Detecting inclusions in electrical impedance tomography without reference measurements," *SIAM J. Appl. Math.*, vol. 69, no. 6, pp. 1662–1681, 2009.

[52] S. Schmitt, "The factorization method for EIT in the case of mixed inclusions," *Inverse Problems*, vol. 25, no. 6, p. 065012, 2009.

[53] B. Harrach, J. K. Seo, and E. J. Woo, "Factorization method and its physical justification in frequency-difference electrical impedance tomography," *IEEE Trans. Med. Imaging*, vol. 29, no. 11, pp. 1918–1926, 2010.

[54] S. Schmitt and A. Kirsch, "A factorization scheme for determining conductivity contrasts in impedance tomography," *Inverse Problems*, vol. 27, no. 9, p. 095005, 2011.

[55] B. Harrach, "Recent progress on the factorization method for electrical impedance tomography," *Comput. Math. Methods Med.*, vol. 2013, 2013.

[56] B. Harrach and M. Ullrich, "Monotonicity-based shape reconstruction in electrical impedance tomography," *SIAM J. Math. Anal.*, vol. 45, no. 6, pp. 3382–3403, 2013.

[57] A. Tamburrino and G. Rubinacci, "A new non-iterative inversion method for electrical resistance tomography," *Inverse Problems*, vol. 18, pp. 1809–1829, 2002.

[58] A. Tamburrino, "Monotonicity based imaging methods for elliptic and parabolic inverse problems," *J. Inverse Ill-Posed Probl.*, vol. 14, pp. 633–642, 2006.

[59] A. Tamburrino, S. Ventre, and G. Rubinacci, "Recent developments of a monotonicity imaging method for magnetic induction tomography in the small skin-depth regime," *Inverse Problems*, vol. 26, no. 7, p. 074016, 2010.

[60] E. Somersalo, M. Cheney, and D. Isaacson, "Existence and uniqueness for electrode models for electric current computed tomography," *SIAM J. Appl. Math.*, vol. 52, no. 4, pp. 1023–1040, 1992.

[61] M. Ikehata, "Size estimation of inclusion," *J. Inverse Ill-Posed Probl.*, vol. 6, no. 2, pp. 127–140, 1998.

[62] H. Kang, J. K. Seo, and D. Sheen, "The inverse conductivity problem with one measurement: stability and estimation of size," *SIAM J. Math. Anal.*, vol. 28, no. 6, pp. 1389–1405, 1997.

[63] B. Harrach and J. K. Seo, "Exact shape-reconstruction by one-step linearization in electrical impedance tomography," *SIAM J. Appl. Math.*, vol. 42, no. 4, pp. 1505–1518, 2010.

[64] A. Lechleiter and A. Rieder, "Newton regularizations for impedance tomography: convergence by local injectivity," *Inverse Problems*, vol. 24, p. 065009 (18pp), 2008.

[65] M. K. Choi, B. Harrach, and J. K. Seo, "Regularizing a linearized EIT reconstruction method using a sensitivity-based factorization method," *Inverse Problems in Science and Engineering*, no. ahead-of-print, pp. 1–16, 2013.

[66] D. Miklavčič, N. Pavšelj, and F. X. Hart, "Electric properties of tissues," *Wiley encyclopedia of biomedical engineering*, 2006.

[67] T. Vilhunen, J. Kaipio, P. Vauhkonen, T. Savolainen, and M. Vauhkonen, "Simultaneous reconstruction of electrode contact impedances and internal electrical properties: I. Theory," *Meas. Sci. Technol.*, vol. 13, no. 12, pp. 1848–1854, 2002.